

Development of Multimodal Quantitative MRI Techniques to Assess Brain Tissue Microstructure in Multiple Sclerosis

Mathieu Boudreau

Supervisor: Bruce Pike

PhD Progress Meeting

Biomedical Engineering Department

McGill University

FINAL - 11/18/13 10:42 PM

1. Introduction and Objectives

Multiple sclerosis (MS) is arguably the most disabling chronic neurological disease affecting a sizable portion of young adult Canadians. While the trigger of the disease is still unknown, considerable efforts have been made in the last few decades at investigating the progression of the pathology of MS. Magnetic resonance imaging (MRI) has emerged as an important imaging modality for diagnosing MS by detecting MS lesions and, in some instances, measuring multiple aspects of the disease. Some techniques provide mostly qualitative features such as T₂ weighted images, but more recently quantitative measures of myelin and water content have been achieved with novel MRI techniques such as quantitative magnetization transfer (qMT) imaging and quantitative T₂. Until now, most of the effort at characterizing MS with MRI has concentrated on white matter (WM) pathology, but recent post-mortem studies have emphasized the importance of cortical grey matter (GM) pathology to fully characterize the disease. **In this thesis, we aim to develop a fast high-resolution whole-brain quantitative magnetization transfer method capable of characterizing white and gray matter MS pathology and to investigate the spatial relationship between pathology in both tissues.**

2. Abbreviated Literature Review

2.1 Multiple Sclerosis

Canada has one of the highest occurrences of MS in the world. MS occurs mostly in women, with clinical onset typically beginning between ages 15-40 (1) and burdens the patient for their entire lifetime. MRI plays a crucial role in the diagnosis of MS, as described by the McDonald Criteria (last revised in 2010) (2). The most common type of MS is conventionally characterized as intermittent attacks of focal WM inflammation and demyelination (plaques), separated by periods of relative stability (3-5). Demyelination in MS WM is believed to be a result of an immunologically mediated attack on myelin and oligodendrocytes (4). Although MS has mostly been described as a WM disease, post-mortem histological evidence has shown many abnormalities in cortical GM of MS patients (6,7). GM lesions are characterized by demyelination, axonal and dendritic transection, neuronal apoptosis and limited inflammatory cell content compared to WM lesions (8-12). One post-mortem study observed that 26% of MS lesions involved some GM (13). Another recent study reported that cortical GM pathology significantly correlated with neurological impairment in relapse-remitting MS patients (14). Despite this, most MRI techniques currently in use concentrate on WM lesions. The development of MRI methods capable of quantifying cortical GM pathology is important to fully characterize MS.

2.2 Magnetic Resonance Imaging of MS

MRI is well known to be very sensitive to various pathologies related to MS (2,7,15-21). The conventional MRI characteristic of MS is hyperintense signals in T₂-weighted MRI of multiple focal WM lesions. However, T₂ hyperintensity has little specificity to the lesion environment, as multiple pathological changes such as acute inflammation and axonal loss can lengthen T₂. Conventional MRI also does not detect the full extent of MS pathology in regions referred to as normal appearing white matter (NAWM) and cortical GM. Brain atrophy, a common disease progression indicator for many neurological diseases such as MS, can also be quantified using MRI (14,22-25).

Cortical GM lesions typically elude MRI detection with clinical MRI scans (26,27). New techniques such as double inversion recovery (DIR) have shown better detection of cortical lesions. DIR uses two inversion pulses that null both WM and CSF, ideally leaving mostly GM signal (28).

However, low SNR and CNR of DIR limit the detection of subtle cortical lesions, such as Type 3 subpial lesions.

2.3 Quantitative MRI

Quantitative MRI techniques, such as quantitative T₁, T₂, diffusion, and magnetization transfer, have become the focus of research development for MS due to their promise of providing hardware and site independent MRI measures and better MS diagnostic specificity (29). MT measures have been shown to strongly correlate with myelin content in brain white matter (16,17), and it is expected that a similar correlation with grey matter can be observed if resolution and SNR is improved (20). Diffusion MRI can be used to trace the fiber connections in the brain with tractography. Multiple axon orientations within an image voxel are difficult to resolve with diffusion tensor imaging, but recent advancements such as high angular resolution diffusion imaging (HARDI) and diffusion spectrum imaging (DSI) provide improved fiber tracking in areas of fiber crossing and branching (30-33). Changes in diffusion MRI metrics such as radial diffusivity can also characterize MS lesion (34-36).

2.4 Magnetization Transfer

Magnetization transfer (MT) is the MR phenomenon of nuclear spins in different environments exchanging magnetization through coupled relaxation (37-40). This method provides an indirect measurement of hydrogen in a semi-solid macromolecular state, as signal from these molecules is undetected with conventional MRI due to the characteristic fast signal decay of solids. This technique provides an indirect measurement of relative semi-solid (e.g. myelin) density. Although MT has been mostly used to investigate multiple sclerosis, other applications include HIV (41-43), Alzheimer's disease (44-47), and articular cartilage (48,49).

The most simple and common magnetization transfer metric is the magnetization transfer ratio (MTR), which consists of two measurements: one with and one without an off-resonance saturation pulse. Although MTR has been shown to correlate with T₁/T₂ weighted MRI images and histology (16), quantitative methods using mathematical models of the magnetization transfer (38,50-54) can provide a more quantitative analysis of the disease. Schmierer et al. (17) compared qMT measurements with quantitative histology on post-mortem MS brains and observed that myelin density was strongly correlated with the restricted pool size ratio (F), and that F could distinguish between normal appearing WM and remyelinated WM lesions; however, cortical pathology was not examined. qMT MRI protocols have historically suffered from very long acquisition times due to the large number of measurements typically required. Several developments have been introduced to overcome this limitation, such as optimal sampling schemes (55,56), reduced sampling by parameter restricting (57,58) and novel qMT re-interpretations of rapid pulse sequences (59).

2.5 Compressed Sensing

Compressed sensing is an image compression technique whose underlying principles have recently been applied to MRI to accelerate image acquisition (60). It allows k-space data to be sampled below the Nyquist criteria while preserving image fidelity and SNR, and does not require major changes to MRI pulse sequence or new hardware. The basic idea behind compressed sensing is the following: **sparse signals may be accurately reconstructed from random k-space undersampling by solving a non-linear optimization problem.** There has been a rapid growth of the use of compressed sensing in the MRI community, with applications ranging from angiography (60), cardiac imaging (61) and diffusion spectrum imaging (62). Several model-based compressed sensing methods have been introduced to take advantage of sparsity in the parameter acquisition domain (63-65).

Bayesian analysis has also been used for simultaneous multi-contrast compressed-sensing reconstruction (66,67). Lastly, an important branch of compressed sensing is the development of methods for multi-coil receivers (68-76).

3. Reminder of Thesis Hypotheses

The major limitations to widespread use of the Sled and Pike qMT method is its very long acquisition times and single-slice acquisition. The low resolution of the protocol ($2 \times 2 \times 7 \text{ mm}^3$) also limits the confidence in cortical pathology measurements using this method. *The next logical step is to develop a high-resolution whole-brain 3D qMT protocol able to confidently characterize cortical pathology in addition to white matter so that fundamental questions on the spatial progression of pathology in MS may be answered.* Our research plan is driven by the following hypotheses/questions:

1. *Quantitative MT acquisitions can be optimized for both white and grey matter sensitivity over the whole brain with a resolution of 1 mm^3 in a clinically acceptable time of <30 minutes.*

Our current qMT protocol is based on a single-slice spoiled gradient recalled echo (SPGRE) sequence with many MT pulse power/offset/frequency/repetition time combinations. We will optimize our method for high resolution (1 mm^3) whole-brain measurements at 3 T using a 32-channel head coil, optimal sampling scheme for normal/MS tissue properties at 3 T, and a novel compressed sampling imaging method to undersample k-space without losing integrity of the qMT maps.

2. *High-resolution quantitative MT WM/GM focal and diffuse pathology in a post-mortem MS brain will correlate with quantitative histology measurements of pathology.*

The next logical step will be to evaluate our optimized qMT protocol in post-mortem MS brains and compare with high-resolution data ($350 \mu\text{m}$ isotropic) and quantitative immunohistochemistry.

3. *Is cortical GM MS pathology spatially independent of connectivity with WM lesions?*

There are substantial differences between cortical and WM MS lesions; for example, cortical lesions exhibit reduced T-cell and B-cell infiltration and gliosis (8). Some suggest that certain GM lesions may be degenerative and secondary to WM lesions (24). This hypothesis will be investigated by combining our new qMT protocol with tractography in a study of secondary progressive MS patients.

4. Progress Since Comprehensive Exam

4.1 Quantitative Comparison of B_1 Mapping Methods for White Matter T_1 Mapping at 3T (Work for Aim 1)

At the ISMRM 2013 meeting, I was approached by Dr. Christine Tardif, a lab alumni, to see if there was interest in a collaboration to continue a project she began in 2011 – a comparison between several B_1 methods on VFA T_1 values, which she had already investigated in phantoms. This work fitted well in my Aim 1, as accelerating the acquisition time of the complete qMT protocol for high-resolution 3D whole-brain imaging will require rapid B_1 mapping techniques such as Actual-Flip-Angle Imaging (AFI) (77,78) or Bloch-Siegert (BS) (79). The aim of this work was to compare VFA T_1 maps in white matter (WM) produced with four B_1 methods: Reference double angle (DA), Bloch-Siegert, Actual Flip-Angle Imaging, and DA using a stock scanner spin-echo EPI readout sequence (EPI-DA).

Prior to acquiring a set of subject data, several technical developments were made. Quantitative maps (B_1 , T_1) processing code were standardized and integrated into an automated Matlab pipeline using MINC and Niak. Our old custom Bloch-Siegert sequence, which performed poorly in Dr. Tardifs ISMRM 2011 work using a Gaussian off-resonance pulse (80), was updated to use off-resonance Fermi pulse, in accordance with the parameters reported in the original paper (79). A majority voting analysis resampling script was developed to resample high-resolution tissue classification maps (WM, GM, CSF) provided via INSECT with the ICBM-152 atlas, to the low resolution (2x2x5 mm³ slice) that the quantitative maps will be acquired.

Six healthy adult subjects were scanned with a 3T Siemens Tim Trio MRI using a 32-channel receive-only head coil. Axial slices (2x2x5 mm³) were acquired (or extracted from 3D volumes) parallel to the AC-PC line above the corpus callosum. Single slice B_1 maps and WM T_1 maps for a single subject are shown in Fig. 1. Figure 2 compares reference DA and EPI-DA sagittal B_1 maps for a single subject. No significant B_1 maps distortions were observed in axial or sagittal EPI-DA B_1 maps. Linear regression analysis of pooled WM T_1 for each B_1 relative to the reference is shown in Figure 3. All B_1 methods provided comparable B_1 and VFA T_1 maps. EPI-DA, the fastest of the B_1 maps (5 s/slice), had no observable distortion artefacts (Figs. 1 and 2), due to careful sequence planning (low EPI factor, long echo spacing). Strong correlations were observed between VFA T_1 maps using all three rapid methods compared to Ref. DA (Figure 3). This work was submitted in November to the ISMRM 2014 conference (Appendix A).

4.2 Effect of Different T_1 Mapping Techniques on a Quantitative Magnetization Transfer MRI Biomarker for Myelin Density (Work for Aim 1)

This work was a continuation of some qMT simulations done last year, which investigated the effects of different T_1 methods on qMT fitted parameters (Fig. 4). To reduce the total acquisition time of the qMT protocol for high-resolution 3D volumes, the conventional LL T_1 measurements must be replaced by a rapid T_1 technique, such as the Variable Flip Angle T_1 technique. A recent comparison (Appendix E) between three commonly used T_1 techniques (inversion recovery - IR, Look-Locker - LL and variable flip angle - VFA) showed significant disagreement in values in white matter (WM). This study investigated the effects of different T_1 techniques on qMT parameters in WM of healthy subjects.

A preliminary *in vivo* MRI study comparing the effect of three T_1 methods on qMT was performed on one healthy female (age 27), and was submitted to the endMS Conference 2013 (Appendix B, accepted for a poster). The protocol consisted of T_1 maps acquired from IR, LL and VFA scans, a pulsed qMT acquisition protocol optimized for 3T, a structural MPRAGE, and additional scans required for qMT processing (B_0 , B_1). Four periventricular ROIs were selected from a single slice above the ventricles, bilaterally in the frontal and occipital lobes. The mean qMT F value using IR T_1 data was 0.14 ± 0.02 (n.u.). Relative to IR, mean F values fitted with LL and VFA T_1 maps were 16% higher and 12% lower respectively.

Six additional healthy adult subjects were scanned as part of the protocol for the study described in Section 4.1. Pooled histograms (all subjects) for all qMT parameters (WM masked) are shown in Fig. 5. The overestimation in VFA T_1 values deviated F away from IR less than for LL. Scaling the whole brain VFA T_1 values with the use of single slice IR T_1 values could be explored to reduce the shift in F values, although the histogram broadening apparent in VFA may still be present.

4.3 Insensitivity of B_1 on our qMT Protocol (Work for Aim 1)

Over the course of analyzing the data acquired discussed in Sections 4.1 and 4.2, an unexpected result (very high correlations of pooled F values for all B_1 methods when using VFA T_1 data)

motivated some additional analysis, which led to a second ISMRM abstract (Appendix C) that was submitted in November.

Quantitative magnetization transfer (qMT) imaging requires several additional measurements to correct for instrumental biases (B_0 , B_1) and to constrain parameters in the fitting model (T_1). These three extra measurements are typically independent of each other, but certain T_1 mapping techniques also require B_1 maps (e.g. variable flip angle – VFA). In this case, B_1 is used twice before fitting the qMT parameters: to correct the flip angles for T_1 mapping, and to scale the nominal MT saturation powers. Inaccuracies in B_1 would propagate to the fitting of the qMT parameters through two pathways – through errors induced in T_1 , and errors in MT saturation powers. This work demonstrated that for the Sled and Pike qMT model, certain qMT parameters (F – pool ratio, and T_{2f}) are insensitive to a large range of B_1 inaccuracy when using VFA for T_1 mapping.

VFA and IR T_1 maps were acquired using the same protocols used in Sections 4.1 and 4.2. MT data was acquired using the spoiled gradient echo two-TR (25/60 ms) optimal 10-point protocol for 3T using Gaussian-Hanning MT pulses. A double angle (DA) B_1 map was acquired using the same protocols used in Sections 4.1 and 4.2. To simulate a wide range of B_1 inaccuracies, flat (homogenous) B_1 maps were simulated for a range of values (B_1 Flat = between 0.5 and 2 n.u.). VFA T_1 maps and corrected MT saturation powers were then calculated from these flat B_1 maps to provide a wide range of inaccurate T_1 and MT saturation powers. Note that VFA T_1 calculated with a flat B_1 factor of 1 is equivalent to fitting VFA T_1 maps using the nominal flip angles. qMT maps were fitted with combinations of B_1 maps using DA and flat B_1 , as well as IR T_1 maps and VFA T_1 maps corrected with the corresponding B_1 maps. Figure 6 shows a comparison between B_1 maps (measured DA and simulated B_1 flat = 1, the latter being equivalent to assuming true nominal angles) for a single subject; VFA T_1 maps calculated using each B_1 map; and fitted qMT F maps. Figure 7 shows the pooled whole brain Pearson correlation coefficients (a) and linear regression slopes (b) for qMT F values between the measured DA B_1 maps and simulated flat B_1 maps, for VFA (blue) and IR (red) T_1 maps.

As can be observed from Fig. 6, processing qMT F maps using a flat B_1 map (nominal flip angle assumption, large B_1 inaccuracies) and the corresponding VFA T_1 map results in nearly identical qMT F maps using DA B_1 maps. The exact origin of the erroneous B_1 , and subsequently VFA T_1 , nearly cancelling out in qMT F maps remains to be clarified, and simulations may provide a better understanding this insensitivity. The results of this work implies that B_1 mapping could be completely eliminated from our qMT protocol with no undesired biases on F by using VFA for T_1 maps, which could save up to 10 minutes from our 3D qMT protocol acquisition time.

4.4 qMT Compressed Sensing (Work for Aim 1)

The compressed sensing k-space acceleration part of Aim 1 has undergone some technical developments over the course of this year, but is still a work in progress. Sparse k-space pulse sequence acquisition was developed with the aid of the newly hired Montreal Siemens collaboration scientist, Dr. Raphaël Paquin. The method was successfully developed to the stock Siemens 2D gradient echo pulse sequence (the base sequence for our qMT sequences), with the capability of reading the k-space lines to be acquired from a text file, allowing for great at-the-scanner flexibility. This feature will be extended to 3D and merged with our qMT sequence in the next few months. To aid in this transition, an additional feature to the qMT sequence was developed to allow single point acquisitions instead of full qMT protocols, and user interface MT parameter control (MT saturation, off-resonance frequency). Additionally, as raw (k-space) data from all 32 channels must be used for compressed sensing, Matlab code was developed to organize the loaded raw data into k-space and/or image domain matrices using the measurement data headers. Lastly, an open source L_1 -SPIRIT (68,70) multi-channel sparse

acquisition image reconstruction software package was installed and tested on one of our lab computers. This software significantly accelerates multi-channel L1-Spirit processing through the use GPU processing (through NVIDIA's CUDA toolkit) or OpenMP multi-processor tools.

4.5 Other – Training

Throughout this year, I had the opportunity to participate in several training programs, both technical and career-oriented. In February, I completed a weeklong course IDEA Sequence Programming offered by Siemens Training and Development. This course covered pulse sequence design and philosophy, real time event programming, testing software utilization, and software programming tools. The abstract submitted last year at ISMRM was accepted as a traditional poster, and I was awarded an ISMRM Trainee Educational Stipend to attend the meeting and the weekend educational course that preceded the meeting. The McGill Biomedical Engineering Department GREAT Travel Award (Graduate Research Enhancement and Travel Award) also provided funding to attend the meeting. Lastly, I received a competitive scholarship to attend this year's weeklong endMS Research and Training Network Summer School. This summer school covered a range of topics, such as imaging and pathogenesis of MS, discussions with MS and neuromyelitis optica (NMO) patients, ethics workshops, clinical trials, effective communication techniques, and media relations.

5. Upcoming Research Plan

5.1 Aim 1: qMT Compressed Sensing

The next step in the completion of Aim 1 of this thesis will be to establish a compressed sensing image reconstruction technique for our qMT pulse sequence. This will be done in collaboration with Dr. Ives Levesque, an alumni of Dr. Pike's lab, and a medical imaging physicist who has recently joined McGill University as an assistant professor at the McGill University Health Center. Dr. Levesque has several years of experience in developing compressed sensing techniques for quantitative imaging methods. We have met on several occasions this fall to discuss this project.

The first step will be to investigate the sensitivity of each qMT Z-spectrum acquisitions to compressed sensing related artifacts that propagate into the final qMT fitted parameter maps. This will be investigated using the open source L₁-SPIRIT+Wavelet reconstruction processing code mentioned in Section 4.4. K-space data will be retroactively undersampled at different acceleration factors for each qMT point, then each point will be individually reconstructed and fitted for qMT parameters with the other fully sampled qMT points. Raw single slice (2x2x5 mm³) k-space data (fully acquired) of our optimal 10-point qMT protocol has already been acquired for 5 healthy subjects as part of another study (Sections 4.2 and 4.3). A fully acquired whole brain (2x2x2 mm³) qMT data set of an MS patient will be acquired in early December 2013 by two Pike lab members (Dr. Nikola Stikov and Dr. Jennifer Campbell), and will generously be sharing the raw data. The patient is a 38 year old male subject with definite relapse-remitting MS (RRMS), EDSS 3.0; recent attacks: Feb 2011, August 2012; treated with Avonex from Jan 2011 - August 2011, as of Aug 2011, he has been treated with Gilenya. This data set will be helpful in evaluating compressed sensing artefacts that may result in the loss of lesion information in fitted qMT maps.

Once the L₁-SPIRIT qMT acquisition sensitivity has been established, an alternative compressed sensing method developed for quantitative parameter mapping using locally low rank constraints (81), will be evaluated for qMT and compared to our L₁-SPIRIT analysis. This is work that Dr. Levesque is intimately familiar with, having supervised a PhD student who made significant developments in this method, and has access to processing code that have been developed at Stanford University by Tao Zhang. This method takes advantage of the data redundancy in the MRI parameter

domain (e.g. for T_2 measurements, the parameter being varied is TE) through sparsity in the singular values of a Casorati matrix (column is the image voxel dimension, row is the parameter dimensions). This method is a model-free parameter-domain compressed sensing method, and may promise to be more efficient at accelerating acquisition than the L_1 -Spirit method, which does not take into account of parameter domain redundancy. The comparison and optimization of these two methods using qMT could comprise of a technical note or full paper.

5.2 Aim 1: Completion of ISMRM 2014 Abstract Work

The work for Aim 1 completed until now has resulted in 3 conference abstract submissions (2 – ISMRM 2014, 1 - endMS Conference 2013). I hope that with some additional work, either of the ISMRM abstracts could be published as a technical note in a journal such as Magnetic Resonance in Medicine or Journal of Magnetic Resonance Imaging.

The measurements for the qMT abstract (Section 4.3) demonstrated that for our qMT model, the qMT F parameter is insensitive to a large range of B_1 inaccuracy when using VFA for T_1 mapping. The exact origin of the erroneous B_1 and VFA T_1 nearly cancelling out in qMT F maps remains to be clarified, and simulations may provide a better understanding this insensitivity. These simulations will be done using the qMT simulation and fitting code that is already in use in our lab, and will be done at the same time as the work described in Section 5.1.

For the project comparing the quality of VFA T_1 maps using different B_1 methods, additional work may be done to evaluate if sinc interpolations or blurring could improve consolidating all B_1 method, for example by removing some visible anatomical regions such as the sulci and ventricles in EPI-DA B_1 maps (Figs. 1 and 2).

5.3 Aim 2: Quantitatively compare MS pathology in post-mortem brains using the optimized whole-brain quantitative MT protocol and immunohistochemistry

We originally planned to begin Aim 2 of this thesis in January 2014. The fast qMT protocol using compressed sensing is not expected to be developed and tested before mid to late spring 2014, thus this project will be delayed until that time. No significant changes to this aim are currently expected; we will evaluate our optimized qMT protocol in post-mortem MS brains and compare with high-resolution data (350 μm isotropic) and quantitative immunohistochemistry (IHC). The relationship between qMT and quantitative IHC measures in normal, normal appearing GM and GM lesions will be statistically evaluated. Results from this aim will provide valuable information on the sensitivity the optimized qMT protocol (Aim 1) to GM MS pathology. We'll begin the process of acquiring ethics approval and processing tissue requests over the course of winter 2014.

5.4 Aim 3: Investigate the spatial relationship between WM and GM MS pathology in a study of secondary progressive MS patients.

No significant change to our original plan for our Aim 3 is currently expected. This work will examine whole-brain cortical GM pathology in MS patients using qMT, and will investigate if cortical regions connected to WM lesions exhibit abnormal qMT parameters compared to contra-lateral regions free of WM lesions.

6. Timeline for Completion of Thesis

6.1 December 2013-May 2014

The target completion date for Aim 1 is May 2014. December 2013 and January 2014 (Aim 1 Phase 1, Fig. 8) will be spent investigating the qMT Z-spectrum point sensitivity on retroactive compressed sensing reconstruction. Healthy subject data ($N = 5$) has already been acquired, and multi-coil L₁-Spirit GPU reconstruction code is already available on one of our lab computers. Compressed sensing reconstructions effect on lesions will be explored with data of a single RRMS MS patient that will be available in mid-December. Locally low rank (LLR) sparsity reconstruction for parameter MRI mapping will be evaluated for qMT in February and March (Aim 1 Phase 2, Fig. 8). If results from the LLR work are fruitful, and demonstrate greater acceleration power than the qMT optimized L1-Spirit method, both will be compared in an in vivo investigation using a sparsely acquired qMT data set of healthy subjects in April and May.

Lastly, simulations exploring the B₁ and VFA T₁ sensitivity on qMT parameters will be done over the course of the first quarter of 2014, to be included in the ISMRM abstract presentation at the 2014 conference, if accepted.

6.2 June 2014-December 2014

During the month of June 2014, the qMT pulse sequence protocol will be adjusted for reductions in post-mortem brains T₁ values due to the fixation process. Post-mortem brain hemispheres (1 healthy, 4 MS for different stages) will be scanned between July and September 2014 during weekends (Aim 2 Phase 1, Fig. 8). Thin sections of the sliced coronal brain slabs will be sent to be immunostained shortly after being scanned. Statistical analysis of MRI and immunohistochemical stains will be performed from October to December 2014. We expect to have sufficient data processed to submit an ISMRM abstract in November.

Additionally, manuscripts for Aim 1 will be written between June and September 2014, overlapping with measurements for Aim 2.

6.3 January 2015-May 2015

As originally planned, Aim 3 will begin after sufficient results from Aim 2 are acquired and interpreted, following our next progress meeting. Secondary progressive MS patient recruitment will begin by January 2015 (Aim 3 Phase 1, Fig. 8). Scanning will be done between January and April 2015. Data will be analyzed overlapping with the months of data acquisition, finishing by May 2015. The manuscript for Aim 2 will be written simultaneous to the measurements for Aim 3, between January and March 2015.

6.4 June 2015 - August 2015

The final manuscript, as well as remaining thesis chapters (Introduction, Background, Conclusion) will be written between June and August 2015. The thesis will be submitted by September 2015.

7. Publications and Conference Proceedings

7.1 Submitted Manuscripts

1. Nikola Stikov, **Mathieu Boudreau**, Ives Levesque, Christine Tardif, Joëlle Barral, G. Bruce Pike, “*On the Accuracy of T₁ Mapping: Searching for Common Ground*”, Submitted to: Magnetic Resonance in Medicine (First submission: August 26th 2013, Second Submission: November 5th 2013)

7.2 Proposed Manuscripts

1. **Mathieu Boudreau**, Nikola Stikov, G. Bruce Pike, “*qMT B_1 Insensitivity when using Variable Flip Angle T_1 Maps*”, Proposed submission to: Journal of Magnetic Resonance Imaging, Format: Technical Note (2014)
2. **Mathieu Boudreau**, Ives R. Levesque, Tao Zhang, G. Bruce Pike, “*Optimized Acceleration of Quantitative Magnetization Transfer Parameter Mapping Using Locally Low Rank Sparsity*”, Proposed submission to: Magnetic Resonance in Medicine, Format: Technical Note (2014)
3. **Mathieu Boudreau**, t.b.d., G. Bruce Pike, “*Cortical Quantitative Magnetization Transfer Imaging in Postmortem Secondary Progressive Multiple Sclerosis Brains*”, Proposed submission to: Magnetic Resonance in Medicine, Format: Full Paper (2015)
4. **Mathieu Boudreau**, t.b.d., G. Bruce Pike, “*On The Spatial Relationship between White and Cortical Grey Matter Lesions*”, Proposed submission to: NeuroImage, Format: Full Paper (2015)

7.3 Accepted Conference Abstracts

1. **Mathieu Boudreau**, Nikola Stikov, G. Bruce Pike, “ *T_1 Mapping: Should We Agree To Disagree?*”, Poster, International Society for Magnetic Resonance in Medicine Meeting 2013
2. **Mathieu Boudreau**, Nikola Stikov, G. Bruce Pike, “*Effect of Different T_1 Mapping Techniques on a Quantitative Magnetization Transfer MRI Biomarker for Myelin Density*”, Poster, endMS Conference 2013

7.4 Submitted Conference Abstracts

1. **Mathieu Boudreau**, Christine Tardif, Nikola Stikov, G. Bruce Pike, “*A Comparison of B_1 Mapping Methods for T_1 Mapping at 3T*”, Submitted to: International Society for Magnetic Resonance in Medicine Meeting 2014
2. **Mathieu Boudreau**, Nikola Stikov, G. Bruce Pike, “*A B_1 Insensitive qMT Protocol*”, Submitted to: International Society for Magnetic Resonance in Medicine Meeting 2014
3. Ye Gu, Nikola Stikov, **Mathieu Boudreau**, Yaaseen Atchia, Ives Levesque, John Sled, G. Bruce Pike, “*qMTLab: An Open Source Software Package for Quantitative Analysis of Magnetization Transfer*”, Submitted to: International Society for Magnetic Resonance in Medicine Meeting 2014

8. Thesis Draft Outline

Chapter 1: Introduction

Motivation for the thesis work will be introduced in Chapter 1. Broad facts about the current knowledge of MS will be discussed at a level accessible to non-experts. Previous MRI limitations leading to the technical developments of this thesis will be discussed. The broad aim of this thesis will be stated.

Chapter 2: Background

Chapter 2 will cover the background required to understand the following integrated articles at level accessible to MS and MRI researchers. White matter MS pathology will be discussed, following by the current state of knowledge of cortical grey matter MS pathology. Quantitative magnetization transfer MRI will be explained in detail, and relevant recent studies will be presented. The compressed sensing technique will be described in detail, and a comparison between methods will be presented.

Chapter 3: (Integrated article, Technical Note) *qMT B_1 Insensitivity when using Variable Flip Angle T_1 Maps*

Chapter 3 will contain the *published* journal article presenting an observed insensitivity of the qMT F parameter to B_1 inaccuracies, when VFA T_1 maps are used. Simulations will be presented to establish the origin and limitations of this observation. MRI measurements of a small set of healthy subjects will be presented, and a comparison double angle and simulated flat B_1 maps, and between VFA and IR T_1 maps, will demonstrate the *in vivo* feasibility of the reported insensitivity.

Chapter 4: (Integrated article, Technical Note) *Optimized Acceleration of Quantitative Magnetization Transfer Parameter Mapping Using Locally Low Rank Sparsity*

Chapter 4 will contain the *published* journal article presenting a parameter-based compressed sensing reconstruction method applied to quantitative magnetization transfer. Single slice healthy subject data will be retroactively undersampled, and each qMT measurement will be individually assessed for sensitivity to L_1 -Spirit compressed sensing artifacts, and a measurement-varying k-space sparse acquisition protocol will be developed. Locally low rank sparsity reconstruction will then be evaluated and compared to the optimal L_1 -Spirit method developed. Lastly, qMT parameter contrast in WM lesions will be compared for both method using data from one (more if available) MS patient.

Chapter 5: (Integrated article, Full Paper) *Cortical Quantitative Magnetization Transfer Imaging in Postmortem Secondary Progressive Multiple Sclerosis Brains*

Chapter 5 will contain the *in press* manuscript that will evaluate our compressed-sensing accelerated qMT protocol in post-mortem secondary progressive MS brains and compare with high-resolution data (350 μm isotropic) and quantitative immunohistochemistry. Thin sections of the sliced coronal brain slabs will be immunostained and digitized for analysis using a fully automated image-processing pipeline to obtain quantitative IHC maps of pathology tissue sections. The relationship between qMT and quantitative IHC measures in normal, normal appearing GM and GM lesions will be statistically evaluated.

Chapter 6: (Integrated article, Full Paper) *On The Spatial Relationship between White and Cortical Grey Matter Lesions*

Chapter 6 will contain the *submitted* manuscript examining whole-brain cortical GM pathology in MS patients using qMT, and will investigate if cortical regions connected to WM lesions exhibit abnormal qMT parameters compared to contra-lateral regions free of WM lesions. The hi-resolution qMT protocol developed in Aim 1 will be combined with tractography in a study of secondary progressive MS patients.

Chapter 7: Conclusion

The final chapter will summarize the thesis work, and provide concise conclusions at a level understandable to non-experts. Future work made feasible due to the technical developments of the thesis will be discussed.

FIGURES

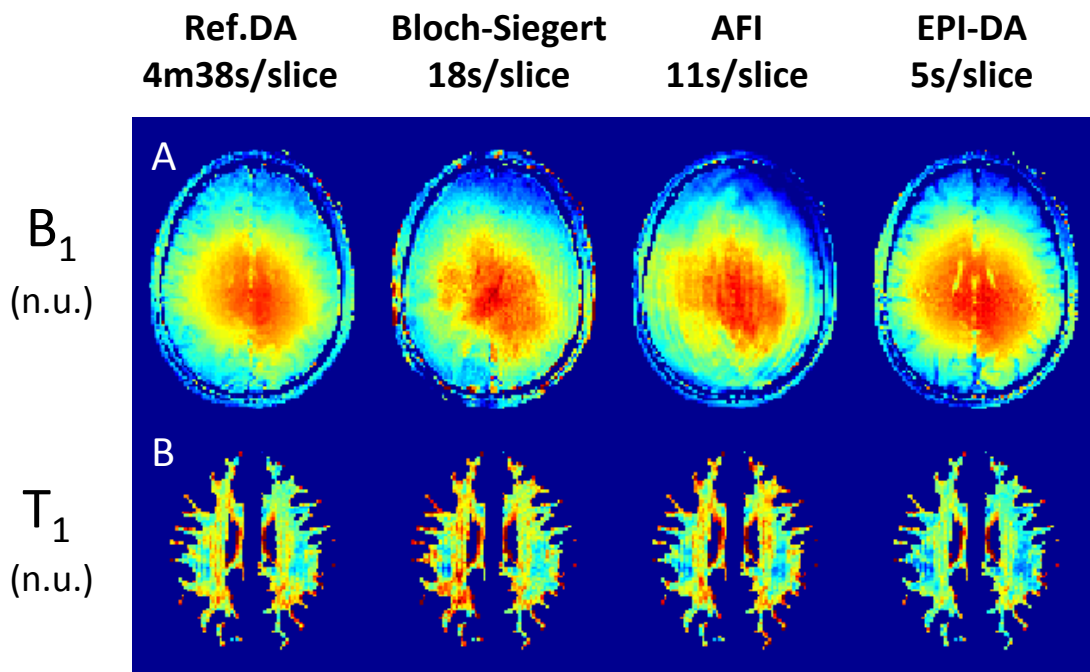


Figure 1: (A) Single slice B_1 maps from a representative subject. (B) WM VFA T_1 maps using flip angles corrected with each B_1 map.

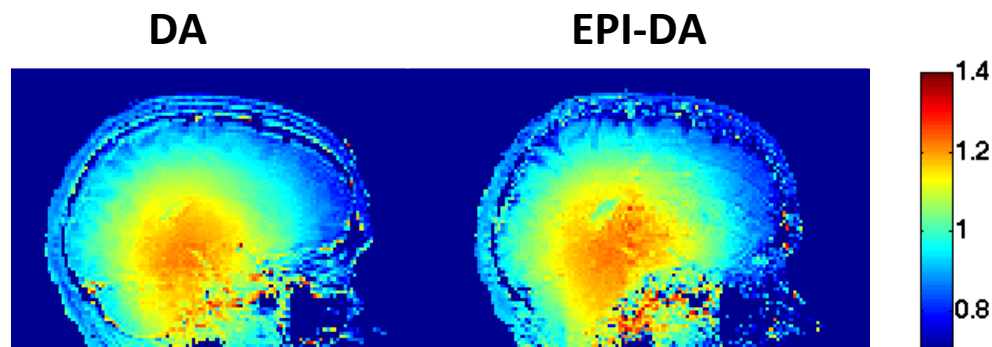


Figure 2: Sagittal (left hemisphere) B₁ maps for a single subject using the reference DA and EPI-DA methods.

| | Ref. DA | BS | AFI | EPI-DA |
|----------------------------------|----------------|-----------|--------------|---------------|
| Pearson ρ | ----- | 0.963 | 0.972 | 0.984 |
| Fit slope | ----- | 0.993 | 1.002 | 0.981 |

Figure 3: Table listing the linear regression analysis of the pooled WM T₁ values (6 subjects) for each B₁ method relative to the reference DA B₁ method.

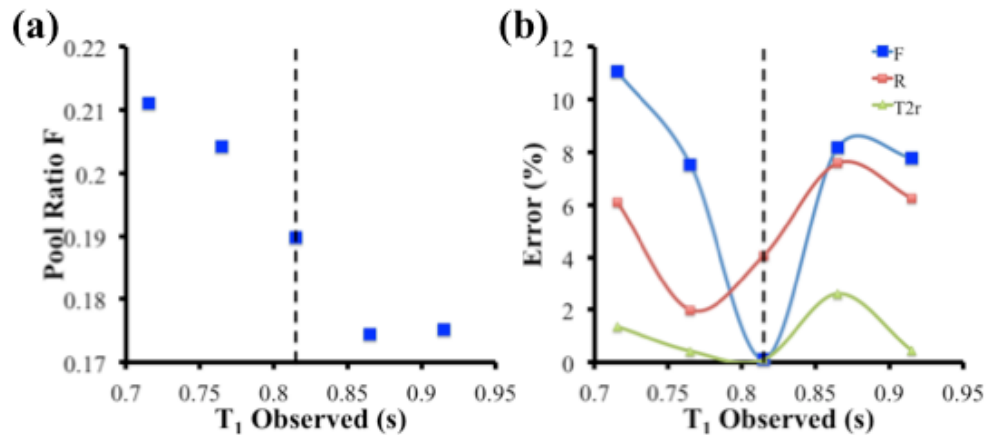


Figure 4. Effect on qMT fitted parameters as a result of measuring a T_1 value different from the true tissue T_1 value (dotted line). (a) Effect on the value of the pool ratio parameter F. (b) The error in fitted parameters for F, R and $T_{2,r}$.

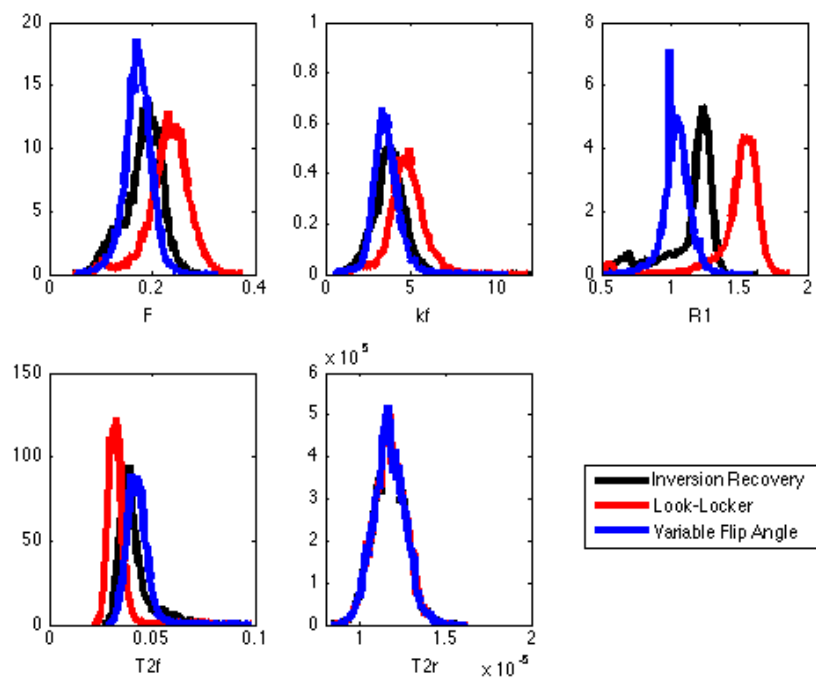


Figure 5: Normalized pooled histograms of single slice WM quantitative MT parameter values for 6 healthy subjects using double angle B_1 maps and IR (black), LL (red), and VFA (blue) T_1 maps.

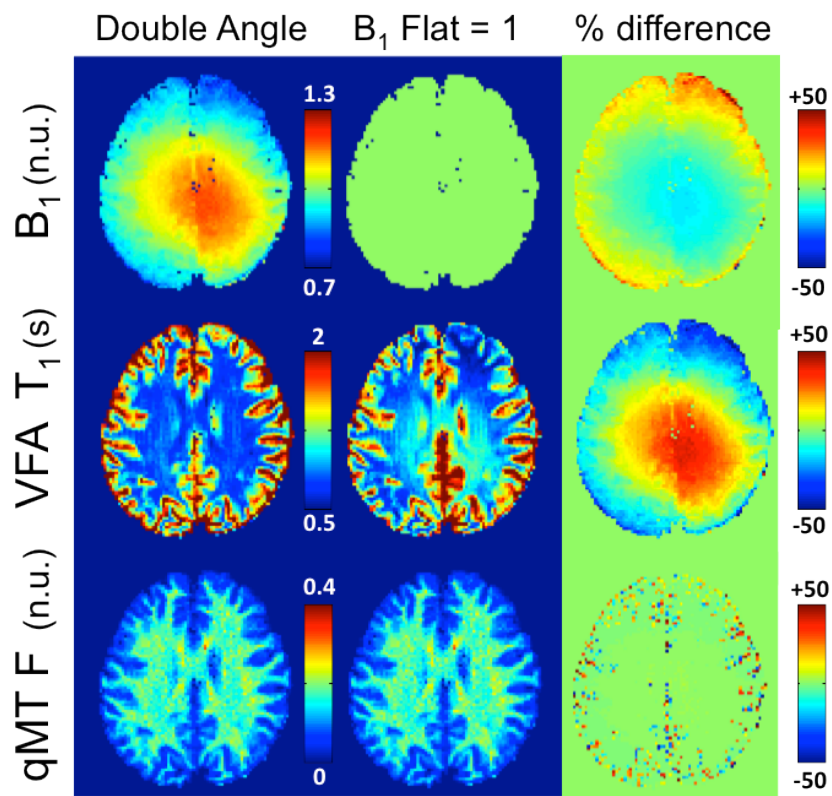


Figure 6: A single subject comparison of qMT F maps fitted using DA and flat ($B_1 = 1$) B_1 maps and VFA T_1 maps corrected using the corresponding B_1 map.

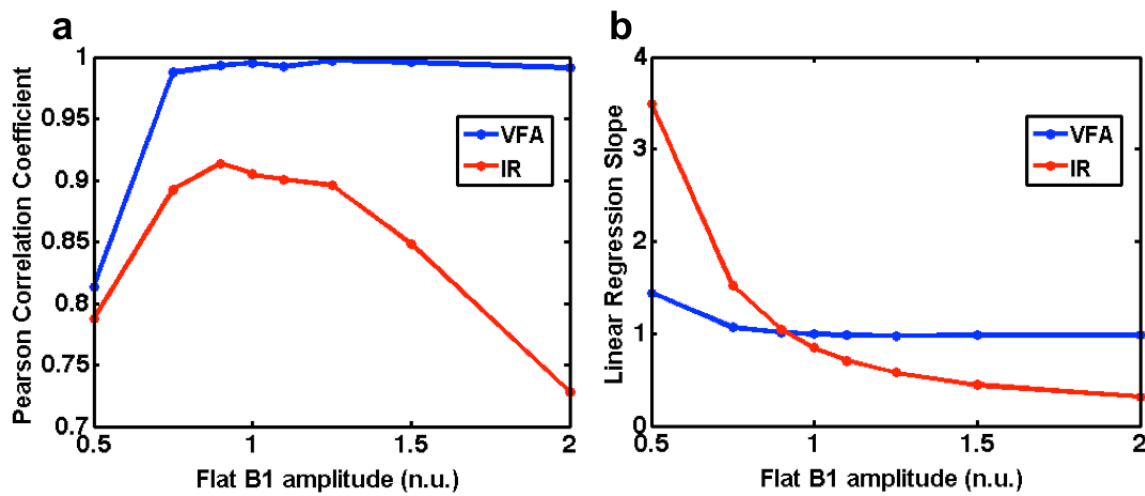


Figure 7: Pooled (all subjects) whole brain Pearson correlation coefficients (a) and linear regression slopes (b) for qMT F values between the measured DA B₁ maps and simulated flat B₁ maps.

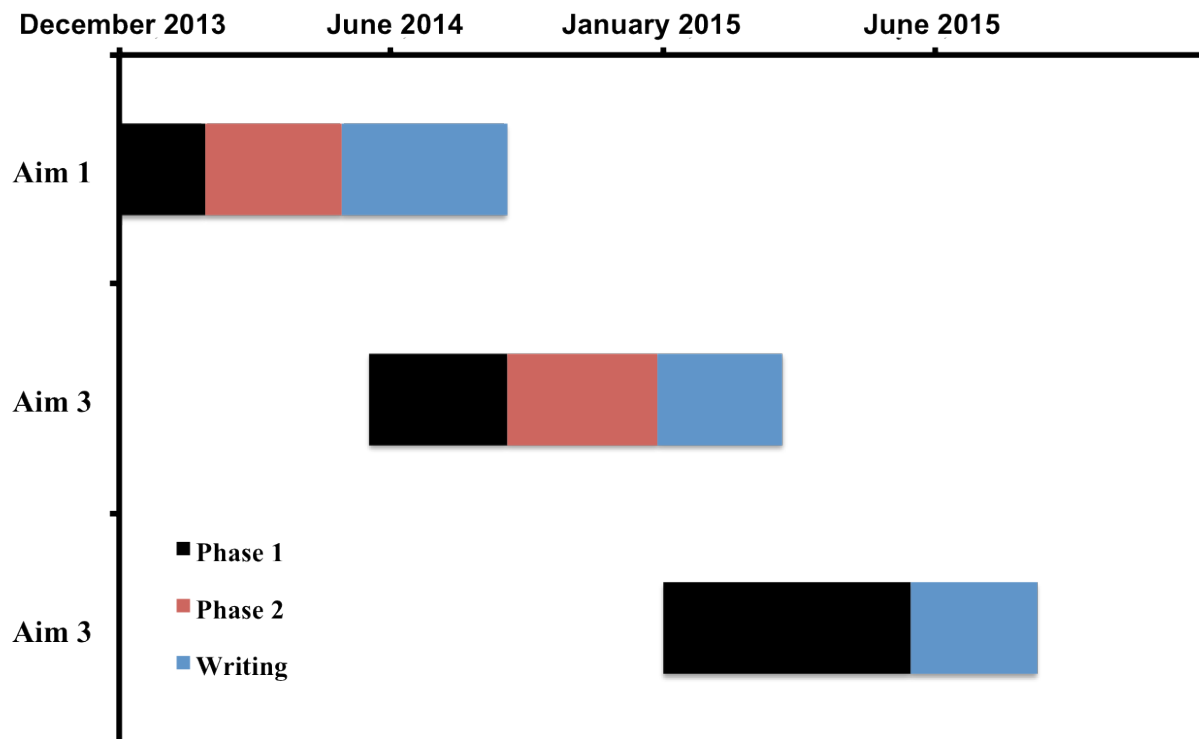


Figure 8. Estimate timeline of the thesis project. Details for each aim are summarized in Section 6 of this document, and in Section 7 of the PhD Thesis Proposal submitted to the McGill Department of Biomedical Engineering in December 2012.

APENDIX A

2014 ISMRM Conference Abstract – 1 (Submitted, 1st author)

1496

A Comparison of B_1 Mapping Methods for T_1 Mapping at 3TMathieu Boudreau¹, Christine Tardif², Nikola Stikov¹, and G. Bruce Pike^{1,3}¹Montreal Neurological Institute, McGill University, Montreal, Quebec, Canada, ²Department of Neurophysics, Max Planck Institute for Human Cognitive and Brain Sciences, Leipzig, Saxony, Germany, ³Hotchkiss Brain Institute, Faculty of Medicine, University of Calgary, Calgary, Alberta, Canada

INTRODUCTION: B_1 maps are an essential part of most quantitative MRI protocols, including Variable Flip Angle (VFA) T_1 mapping. To achieve whole brain quantitative imaging in reasonable scan times, several novel rapid B_1 methods have been introduced^{1,2}. Recent works have compared several novel B_1 mapping methods used at 3T in simulations³, phantoms⁴, and *in vivo*⁵. Accelerating B_1 mapping can also be done through fast k-space trajectories, such as EPI, but are sometimes dismissed due to the possibility of distortions associated artifacts⁶, particularly for brain imaging. The aim of this work was to compare VFA T_1 maps in white matter (WM) produced with four B_1 methods: Reference double angle (DA), Bloch-Siegeert² (BS), Actual Flip-Angle Imaging (AFI), and DA using a stock scanner spin-echo EPI readout sequence (EPI-DA).

METHODS: Six healthy adult subjects were scanned with a 3T Siemens Tim Trio MRI using a 32-channel receive-only head coil. Axial slices ($2 \times 2 \times 5 \text{ mm}^3$) were acquired (or extracted from 3D volumes) parallel to the AC-PC line above the corpus callosum. A reference DA B_1 map was acquired using a turbo spin echo readout with TE/TR 12/1550 ms and $\alpha = 60^\circ/120^\circ$. Whole brain 3D optimally spoiled⁷ AFI B_1 maps were acquired with TE/TR 1.35/20 ms, $N = 5$, $\alpha = 60^\circ$, spoiling gradient moment $A_G = 450 \text{ mT}\cdot\text{ms/m}$ and RF phase increment $\varphi = 39^\circ$. Single slice BS B_1 maps were acquired with TE/TR 15/100 ms, $\alpha = 25^\circ$, 8 ms Fermi Pulse of 500° at $\pm 4\text{kHz}$ off-resonance and $K_{BS} = 74.01 \text{ rad/G}^2$. Interleaved multi-slice spin-echo EPI-DA whole brain B_1 maps were acquired with TE/TR 46/4000 ms, $\alpha = 60^\circ/120^\circ$, EPI Factor = 9 and echo spacing = 4.18 ms. To further investigate possible distortion artefacts in EPI-DA B_1 maps, a left-hemisphere sagittal slice B_1 map for both DA methods was acquired for one subject. VFA T_1 maps were acquired using an optimally spoiled⁷ 3D gradient echo sequence (TE/TR 2.89/15 ms, $\alpha = 3^\circ/20^\circ$, $A_G = 280 \text{ mT}\cdot\text{ms/m}$, $\varphi = 169^\circ$), and the flip angles were scaled voxel-wise by each B_1 map prior to fitting for T_1 . Whole-brain T_1w MPRAGE images ($1 \times 1 \times 1 \text{ mm}^3$) were acquired, and tissue classification maps (WM, GM, CSF) were provided via INSECT⁸ with the ICBM-152 atlas. WM tissue masks were resampled to a $2 \times 2 \times 5 \text{ mm}^3$ slice using a majority voting analysis; GM and CSF were not included because of partial volume effects due to the voxel size.

RESULTS: Single slice B_1 maps and WM T_1 maps for a single subject are shown in Fig. 1. Figure 2 displays histograms for single slice WM T_1 data that was pooled for all subjects. Linear regression analysis of pooled WM T_1 for each B_1 relative to the reference is shown in Table 1. Figure 3 compares reference DA and EPI-DA sagittal B_1 maps for a single subject. No significant B_1 maps distortions were observed in axial or sagittal EPI-DA B_1 maps.

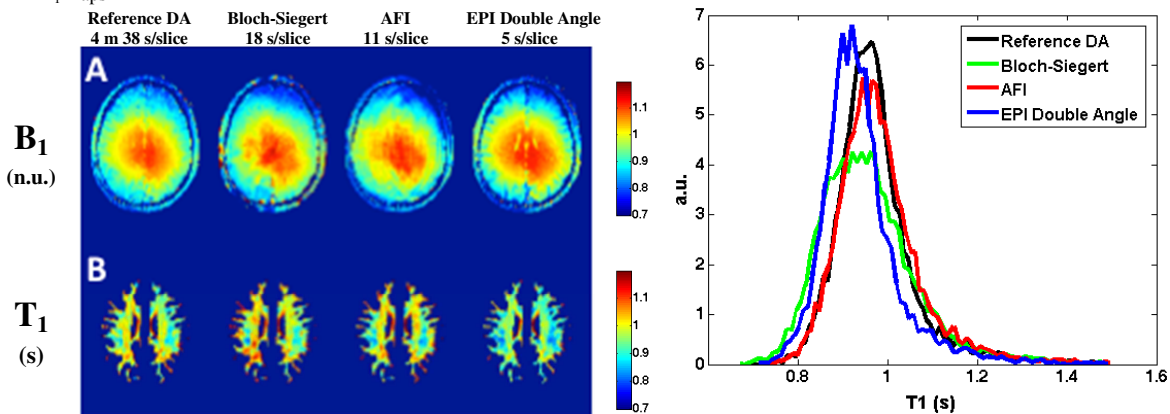


Figure 1: (A) Single slice B_1 maps from a representative subject. (B) WM VFA T_1 maps using flip angles corrected with each B_1 map.

DISCUSSION: All B_1 methods provided comparable B_1 and VFA T_1 maps. EPI-DA, the fastest of the B_1 maps (5 s/slice), had no observable B_1 artefacts (Figs. 1 and 3), due to careful sequence planning (low EPI factor, long echo spacing). Strong correlations were observed between VFA T_1 maps using all three rapid methods compared to Ref. DA (Table 1). T_1 maps using EPI-DA B_1 maps underestimated T_1 by ~4% (Fig. 2., Table 1), but strongly correlated to the Ref. DA.

Transmit B_1 in the brain is typically observed to be a slowly varying function. Interpolating or blurring B_1 maps has been used for both transmit¹ and receive⁶ B_1 , and could remove structural information from the B_1 maps, particularly for maps measured using novel (BS, AFI) or k-space accelerated (EPI-DA) methods. For multi-site or multi-scanner studies requiring whole-brain B_1 maps, EPI-DA could be a good alternative to novel methods, which are not available as stock-sequences on most scanner platforms.

CONCLUSION: All B_1 methods resulted in comparable WM T_1 maps, and all rapid methods strongly correlated with the reference DA map. EPI-DA, the fastest of the techniques derived from a stock scanner sequence, correlated the best with Ref. DA with no observable distortion artefacts. As B_1 maps are expected to be smooth, blurring² or spline smoothing⁹ could be beneficial at improving B_1 maps for quantitative MRI methods (e.g. spline interpolation would remove visible anatomical regions such as the sulci and ventricles in EPI-DA B_1 maps (Fig. 1)).

REFERENCES: [1] Yamykh V., MRM 57:192-200 (2007) [2] Sacolick et al., MRM 63:1610-26 (2010) [3] Sica et al., Proc. Of ISMRM (2010) [4] Tardif et al., Proc. of ISMRM (2010) [5] Lutti A., MRM 64:229-238 (2010) [6] Wade T. and Rutt B., Proc. Of ISMRM (2007) [7] Yamykh V., MRM 63:1610-26 (2010) [8] Collins et al. IPMI 1999, LNCS, Vol. 1613, Springer, Heidelberg 210-223 [9] Sled et al., IEEE Trans. Med. Imag. 17:87-97 (1998)

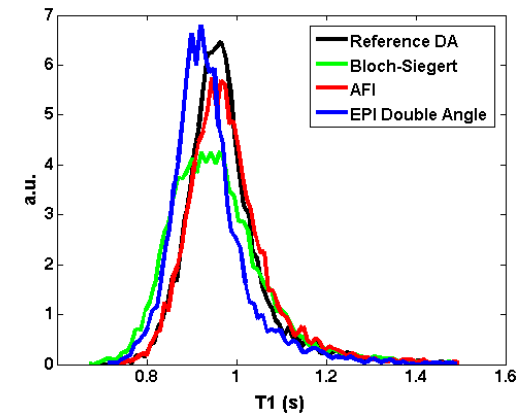


Figure 2: Normalized pooled histograms of single slice WM T_1 values for 6 healthy subjects (bin width = 10 ms).

| | Ref. DA | BS | AFI | EPI-DA |
|-------------|---------|-------|--------------|--------------|
| Pearson p | ----- | 0.963 | 0.972 | 0.984 |
| Fit slope | ----- | 0.993 | 1.002 | 0.981 |

Table 1: Linear regression analysis of the pooled WM T_1 values (6 subjects) for each B_1 method relative to the reference DA B_1 method.

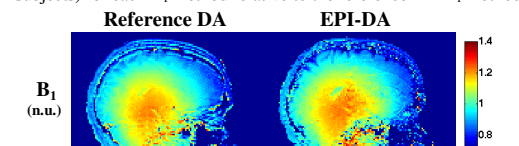


Figure 3: Sagittal (left hemisphere) B_1 maps for a single subject using the reference and EPI double angle methods.

APENDIX B

2013 endMS Conference Abstract (Accepted, first author)

Title: Effect of Different T₁ Mapping Techniques on a Quantitative Magnetization Transfer MRI Biomarker for Myelin Density

Name(s) of author(s): Mathieu Boudreau, Nikola Stikov, G. Bruce Pike

Name of the institution: Montreal Neurological Institute

Objective: Quantitative MRI techniques, such as quantitative T₁, T₂, diffusion, and magnetization transfer (MT), have become the focus of research development for MS due to their promise of providing scanner and site independent MRI measures and better MS pathological specificity. Post-mortem studies in MS patient brains have shown stronger correlation between histological measures of myelin and the quantitative MT (qMT) parameter F (semi-solid to liquid pool magnetization ratio), relative to the MT ratio (MTR). An important requirement for qMT processing is an accurate T₁ map. Recently, a comparison between three commonly used T₁ techniques (inversion recovery - IR, Look-Locker - LL and variable flip angle - VFA) showed significant disagreement in values in white matter (WM). This study investigated the effects of different T₁ techniques on the qMT parameter F, a biomarker for myelin density, in WM of healthy subjects.

Methodology: An in vivo MRI study comparing the effect of three T₁ methods on qMT was performed on one healthy female (age 27). The protocol consisted of T₁ maps acquired from IR, LL and VFA scans, a pulsed qMT acquisition protocol optimized for 3T, a structural MPRAGE, and additional scans required for qMT processing (B₀, B₁). Four periventricular ROIs were selected from a single slice above the ventricles, bilaterally in the frontal and occipital lobes.

Results: The mean qMT F value using IR T₁ data was 0.14 ± 0.02 (unitless). Relative to IR, mean F values fitted with LL and VFA T₁ maps were 16% higher and 12% lower respectively, and their standard deviations were 39% higher and 32% lower. F values for VFA were near the range expected from WM lesions. Lower variance in VFA F values suggests that fewer subjects may be required to achieve acceptable statistical power, but with the calibration of mean T₁ values using an additional IR scan.

APENDIX C

2014 ISMRM Conference Abstract – 2 (Submitted, 1st author)

2431

A B_1 Insensitive qMT ProtocolMathieu Boudreau¹, Nikola Stikov¹, and G. Bruce Pike^{1,2}¹*Montreal Neurological Institute, McGill University, Montreal, Quebec, Canada*, ²*Hotchkiss Brain Institute, Faculty of Medicine, University of Calgary, Calgary, Alberta, Canada*

INTRODUCTION: Quantitative magnetization transfer (qMT) imaging requires several additional measurements to correct for instrumental biases (B_0 , B_1) and to constrain parameters in the fitting model (T_1). These three extra measurements are typically independent of each other, but certain T_1 mapping techniques also require B_1 maps (e.g. variable flip angle – VFA¹). In this case, B_1 is used twice before fitting the qMT parameters: to correct the flip angles for T_1 mapping, and to scale the nominal MT saturation powers. Inaccuracies in B_1 would propagate to the fitting of the qMT parameters through two pathways – through errors induced in T_1 , and errors in MT saturation powers. This work demonstrates that for the Sled and Pike qMT model², certain qMT parameters (F – pool ratio, and T_{2r}) are insensitive to a large range of B_1 inaccuracies when using VFA for T_1 mapping.

METHODS: Three healthy adults were scanned with a 3T Siemens Tim Trio MRI using a 32-channel receive-only head coil. Single slices (2x2x5 mm³) were acquired parallel to the AC-PC line, superior to the corpus callosum. Whole-brain T_1 w MPRAGE images (1x1x1 mm³) were acquired for image registration and skull stripping. **T₁ maps:** VFA T_1 maps were acquired using an optimally spoiled³ 3D gradient echo sequence (TE/TR 2.89/15 ms, $\alpha = 3^\circ/20^\circ$, $A_0 = 280$ mT•ms/m, $\varphi = 169^\circ$), and the flip angles were scaled voxel-wise with each B_1 map prior to fitting for T_1 . Inversion recovery (IR) T_1 data was collected from a four inversion time spin echo sequence (TE/TR = 11/1550 ms, $T_1 = 30, 530, 1030, 1530$ ms), using an open source robust inversion recovery fitting methodology^{4,5}. **qMT maps:** MT data was acquired using the spoiled gradient echo two-TR (25/60 ms) optimal 10-point protocol for 3T using Gaussian-Hanning MT pulses (the full protocol including the 10 off-resonance frequency and MT saturation power pairs can be found in Levesque et al 2011⁶). qMT parameter maps were fitted using the Sled and Pike model². B_1 was mapped using a two-point phase-difference gradient echo method (TE1/TE2/TR = 4/8.48/25 ms). **B₁ maps:** A double angle (DA) B_1 map was acquired using a turbo spin echo readout (TE/TR12/1550 ms, $\alpha = 60^\circ/120^\circ$). To simulate a wide range of B_1 inaccuracies, flat (homogenous) B_1 maps were simulated for a range of values (B_1 Flat = 0.5, 0.75, 0.9, 1, 1.1, 1.25, 1.5, 2 n.u.). VFA T_1 maps and corrected MT saturation powers were then calculated from these flat B_1 maps to provide a wide range of inaccurate T_1 and MT saturation powers. Note that VFA T_1 calculated with a flat B_1 factor of 1 is equivalent to fitting VFA T_1 maps using the nominal flip angles.

qMT maps were fitted with combinations of B_1 maps using DA and flat B_1 , as well as IR T_1 maps and VFA T_1 maps corrected with the corresponding B_1 maps. Voxel data from all subjects were pooled for each qMT/T1/ B_1 sets, and linear regressions and correlations were calculated between qMT/T1/(B₁=DA) and qMT/T1/(B₁ Flat) for all B_1 flat maps and both T_1 methods.

RESULTS: Figure 1 shows a comparison between B_1 maps (measured DA and simulated B_1 flat = 1, the latter being equivalent to assuming true nominal angles) for a single subject; VFA T_1 maps calculated using each B_1 map; and fitted qMT F maps. Figure 2 shows the pooled whole brain Pearson correlation coefficients (a) and linear regression slopes (b) for qMT F values between the measured DA B_1 maps and simulated flat B_1 maps, for VFA (blue) and IR (red) T_1 maps. Table 1 lists the correlation and linear regression slope for all fitted qMT parameters and both T_1 methods (VFA, IR) between DA and B_1 flat = 1.

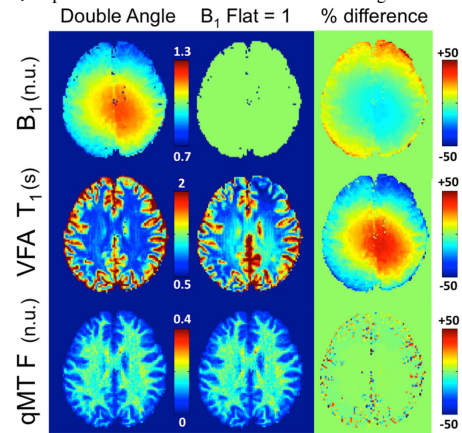


Figure 1: A single subject comparison of qMT F maps fitted using DA and flat ($B_1 = 1$) B_1 maps and VFA T_1 maps corrected using the corresponding B_1 map.

DISCUSSION: As can be observed from Fig. 1, processing qMT F maps using a flat B_1 map (nominal flip angle assumption, large B_1 inaccuracies) and the corresponding VFA T_1 map results in nearly identical qMT F maps using DA B_1 maps, except for cortical regions where partial volume with CSF is present due to the voxel size (2x2x5 mm³). Severe overestimation of B_1 is better tolerated than severe underestimation for the qMT parameter F (Fig. 2). As expected, inaccurate B_1 values lead to severe qMT parameters errors when IR T_1 maps are used (Fig. 2 and Table 1). Poor correlation in R_{1f} values for VFA, and strong correlations for IR R_{1f} (Table 1), can be easily explained because the measured T_1 is used to constrain the fitted R_{1f} ².

The exact origin of the erroneous B_1 and VFA T_1 nearly cancelling out in qMT F maps remains to be clarified, and simulations may provide a better understanding this insensitivity. It may be possible that k_F , which has the lowest correlation (Table 1 – VFA), is absorbing some errors instead of F during the fitting procedure, when the effects of inaccurate B_1 and T_1 compensate each other. F has been observed to be the best qMT correlate with myelin content using histology⁷, and some qMT methods have recently been developed to fix most qMT parameters except F to reduce the number of acquisitions⁸. A likely source of the insensitivity of F and T_{2r} to B_1 may also be that the measured MT signal is inversely proportional to the MT saturation powers, while measured MT signal is proportional to T_1 , and it can be seen from Figure 1 that B_1 and VFA T_1 are inversely proportional. qMT protocols with different TRs or parameter constrained methods⁸ may be more sensitive to B_1 inaccuracies than the protocol presented in this work.

CONCLUSION: We have demonstrated that qMT F maps fitted using VFA T_1 can be insensitive to B_1 inaccuracies. Thus, faster and lower resolution B_1 maps can be used without sacrificing qMT F accuracy or precision when VFA T_1 maps are used. More work in simulating the effects of B_1 and VFA T_1 inaccuracies on qMT parameter estimation is needed to have a clearer understanding of the limitations of this observation.

REFERENCES: [1] Deoni S. et al. MRM 49:515-526 (2003) [2] Sled J. and Pike G. B., MRM 46:923-931 (2001) [3] Yarnykh V., MRM 63:1610-26 (2010) [4] Barral J. et al. MRM 64:1057-1067 (2010) [5] <http://www-mrsrl.stanford.edu/~jbarral/t1map.html> (Accessed: October 2012) [6] Levesque I. et al. MRM 66:635-643 (2011) [7] Schmierer K. et al. JMRI 26:41-51 (2007) [8] Yarnykh V., MRM 68:166-178 (2012)

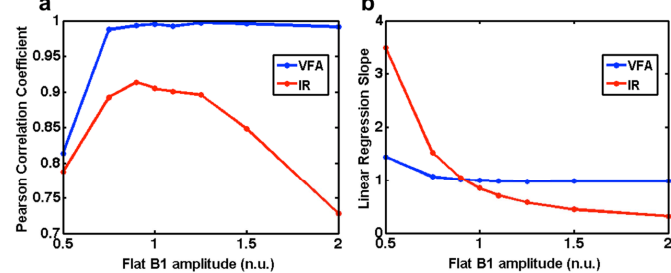


Figure 2: Pooled (all subjects) whole brain Pearson correlation coefficients (a) and linear regression slopes (b) for qMT F values between the measured DA B_1 maps and simulated flat B_1 maps.

| | | F | k_F | R_{1f} | T_{2r} | T_{2r} |
|----------------------------------|-----------|-------------|-------|----------|-------------|----------|
| DA B_1 , VFA T_1 vs | Pearson p | 0.99 | 0.32 | 0.81 | 0.99 | 0.92 |
| | Slope | 0.99 | 0.31 | 0.98 | 0.95 | 0.90 |
| Flat $B_1 = 1$, VFA T_1 vs | Pearson p | 0.90 | 0.36 | 0.99 | 0.96 | 0.90 |
| | Slope | 0.84 | 0.37 | 0.97 | 1.16 | 0.89 |

Table 1: Pooled (all subjects) whole brain Pearson correlation coefficients and linear regression slopes for qMT F values between the measured DA B_1 maps and simulated flat B_1 maps.

APENDIX D

2014 ISMRM Conference Abstract – 3 (Submitted, 3rd author)

3093

qMTLab: An Open Source Software Package for Quantitative Analysis of Magnetization TransferYe Gu¹, Nikola Stikov², Mathieu Boudreau², Yaaseen Atchia³, Ives R Levesque^{4,5}, John Sled^{6,7} and Bruce Pike^{8,9}

¹BioMedical Engineering, McGill University, Montreal, Quebec, Canada, ²Montreal Neurological Institute, McGill University, Montreal, Quebec, Canada, ³Electrical and Biomedical Engineering, University of Toronto, Toronto, Ontario, Canada, ⁴Medical Physics, Oncology and RI-MUHC, McGill University, Montreal, Quebec, Canada, ⁵Radiology, Stanford University, Stanford, CA, United States, ⁶Hospital for Sick Children, Toronto, Ontario, Canada, ⁷Medical Biophysics, University of Toronto, Toronto, Ontario, Canada, ⁸Montreal Neurological Institute, McGill University, Quebec, Canada, ⁹Radiology, University of Calgary, Calgary, Alberta, Canada

TARGET AUDIENCE: MR scientists developing magnetization transfer (MT) imaging and analysis tools, and clinical researchers undertaking MT studies.

PURPOSE: MT imaging is an important tool in the study of tissue composition¹. It is well established that quantitative MT (qMT) offers improved specificity to myelin content, leading to a better understanding of pathology in multiple sclerosis (MS)^{2,3,4,5}. Recent studies have also extended the application of qMT to other fields such as articular cartilage⁶ and cancer tumors⁷. A wide range of qMT techniques are available, which can generally be grouped in two categories, on- and off-resonance qMT^{8,9}. Because of the differences in terminology and pulse sequence implementation, qMT analysis is in need of standardization. A user-friendly, GUI-based software package that includes functionalities for simulation, sensitivity testing, fitting and data processing was built to answer this need. The package, named qMTLab, will be released in the public domain, with the intention to become an open-source standard tool for qMT researchers and users.

METHODS: A GUI based software package was built, using the GUIDE development platform in MATLAB (The MathWorks, Natick USA), for the purpose of simulation, sensitivity testing, fitting, and data processing in the context of qMT. All processing and fitting algorithms – including a approximation method for the *off-resonance* SPGR model – were also developed in MATLAB and are capable of handling MINC, DICOM and MATLAB data. The design concepts were: 1) to develop the entire package in separate modules for different functions (simulation, sensitivity analysis, data handling, processing); 2) to ensure compatibility between modules so that data is easily saved/loaded across modules; and 3) to make the package open-source and design the data structure to allow users to easily design customized protocols and add-ons.

RESULTS: Figure 1 shows on screen of the qMTLab interface, focusing on the single-voxel data fitting module of the package. This module allows users to visualize the behavior of the fitting routine based on the choice of data points and acquisition parameters. Users can fix certain parameters while varying others (shown by A), to perform a quick sensitivity analysis. This module also allows user-generated protocols to be pre-saved and select data points to be used in the fit (shown by B), resulting in a flexible and customizable package. Separate on- and off-resonance modules enable simulation of qMT data sets, and customized data fitting (not shown here). The detailed function of each module is listed in Table 1.

Table 1: Description of the functionality of each module of qMTLab

| Module | On-resonance | Off-resonance |
|--|---|--|
| Bloch equation simulator | Simulate the bSSFP sequences numerically, using the Bloch equations, with a customized combination of qMT parameters. | Uses a two-pool model and Bloch equations with cross-relaxation terms to simulate the effect of any shaped off-resonance MT pulse. |
| Analytical model viewer | Visualize the behavior of the analytical model by varying the qMT parameters. | Visualize the effectiveness of the multi-pulse approximation for given shaped <i>off-resonance</i> MT pulse. |
| Single-voxel fitting and sensitivity analysis | Visualize the sensitivity of the fit to each data range. | Compute and visualize absorption rates and direct effect of customized off-resonance pulse shape. |
| Processing interface | Fit real data using any range of flip-angle and TR. | Create a fitting environment for customized protocols and fit real data. |

DISCUSSION and CONCLUSION: The two main advantages of this software package are its multi-module design and its compatibility with extensions and customizations. The modular framework and the open-source design allow users to easily apply the tools to customized imaging protocols. qMTLab provides a framework for standardizing the validation and fitting of qMT data. The software package will be made freely available¹⁰, at the ISMRM 2014 conference, to the MR community. It is hoped to become a valuable tool for future qMT studies, leading the way toward fast, robust and clinically feasible qMT protocols.

REFERENCES: [1] Wolff and Balaban, Magn. Reson. Med. 10(1):135-144, (1989). [2] Garcia *et al.* Neuroimage 52(2): 532-537, (2010). [3] Schmierer *et al.* J. Magn. Reson. Imaging, 26: 41–51, (2007). [4] Ropele *et al.* American J Neurol: 1-10 (2012). [5] Levesque *et al.* Magn. Reson. Med., 63: 633-640, (2010). [6] Stikov *et al.* Magn. Reson. Med. 66:725-734, (2011). [7] Underhill *et al.* Neuroimage 54(3): 2052-2065 (2010). [8] Sled and Pike. J. Magn. Res. 145(1): 24-36, (2001). [9] Gloor *et al.* Magn. Reson. Med. 45: 265-269 (2008). [10] <https://github.com/sharktank-bic/qMTLab>

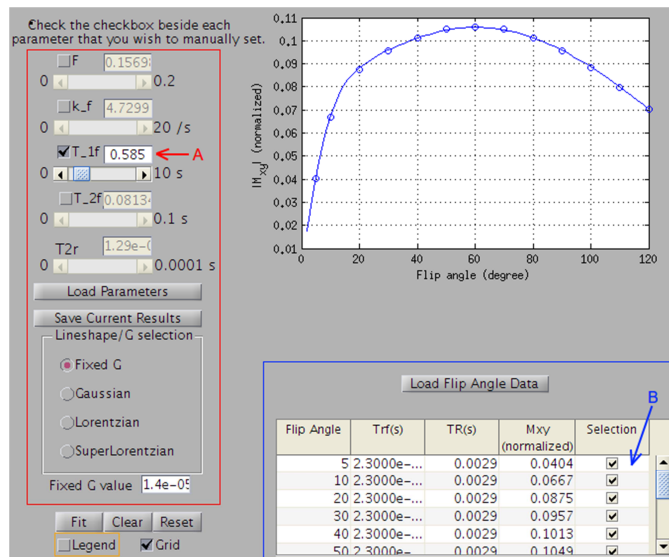


Figure 1: Screenshot of the single-voxel fitting module of the software package. Red square shows parameter setting area. Blue square shows data loading and selection area

APENDIX E

**T₁ mapping article - Magnetic Resonance in Medicine
(Submitted, 2nd author)**

Magnetic Resonance in Medicine

**On the Accuracy of T₁ Mapping: Searching for Common
Ground**

| | |
|-------------------------------|---|
| Journal: | <i>Magnetic Resonance in Medicine</i> |
| Manuscript ID: | MRM-13-14508.R1 |
| Wiley - Manuscript type: | Full Paper |
| Date Submitted by the Author: | n/a |
| Complete List of Authors: | Stikov, Nikola; McGill University, Montreal Neurological Institute Boudreau, Mathieu; McGill University, Montreal Neurological Institute Levesque, Ives; Stanford University, Radiology Tardif, Christine; Max Planck Institute for Human Cognitive and Brain Sciences, Department of Neurophysiology Barral, Joëlle; Stanford University, Electrical Engineering Pike, G; 3801 University St., Neurology/Neurosurgery |
| Research Type: | Relaxation techniques < Technique Development < Technical Research, T1 < Relaxation techniques < Technique Development < Technical Research |
| Research Focus: | No specific tissue or organ focus, Brain < Neurological |
| | |

SCHOLARONE™
Manuscripts

1
2
3
4
5
6
7
8
9

On the Accuracy of T₁ Mapping: Searching for Common Ground

10
11
12
13
14
15
16

Nikola Stikov¹, Mathieu Boudreau¹, Ives R. Levesque², Christine L. Tardif³, Joëlle K.
Barral⁴, G. Bruce Pike¹

17
18
19
20

¹McConnel Brain Imaging Center, Montreal Neurological Institute, McGill University
Montreal, Quebec, Canada

21
22
23

²Department of Radiology, Stanford University, Stanford, CA, USA

24
25
26

³Department of Neurophysics, Max Planck Institute for Human Cognitive and Brain Sciences,
Leipzig, Germany

27
28
29
30
31
32
33

⁴ Department of Electrical Engineering, Stanford University, CA

34
35
36
37

In submission to Magnetic Resonance in Medicine

38
39
40

Contact: Nikola Stikov, PhD

41
42
43

Postdoctoral Fellow
Montreal Neurological Institute
McConnell Brain Imaging Center
3801 University Street, Room WB-325
Montreal, Quebec, Canada
H3A 2B4

44
45
46
47

nikola.stikov@mcgill.ca

48
49
50
51

Word count: 5800

52
53
54
55
56
57
58
59
60

1
2
3
4
5

Abstract:

6
7
8
9
10
11
12
13
14
15
16

Purpose: There are many T_1 mapping methods available, each of them validated in phantoms and reporting excellent agreement with literature. However, values in literature vary greatly, with T_1 in white matter ranging from 690 to 1100 ms at 3T. This brings into question the accuracy of one of the most fundamental measurements in quantitative MRI. Our goal was to explain these variations and look into ways of mitigating them.

17
18
19
20
21
22
23
24
25
26
27

Methods: We evaluated the three most common T_1 mapping methods (inversion recovery, Look-Locker and variable flip angle) through Bloch simulations, a white matter phantom and the brains of 10 healthy subjects (single-slice). We pooled the T_1 histograms of the subjects to determine whether there is a sequence-dependent bias and whether it is reproducible across subjects.

28
29
30
31
32
33
34
35
36
37
38
39
40
41

Results: We found good agreement between the three methods in phantoms, but poor agreement *in vivo*, with the white matter T_1 histogram peak in healthy subjects varying by more than 30% depending on the method used. We also found that the pooled brain histograms displayed three distinct white matter peaks, with Look-Locker consistently underestimating, and variable flip angle overestimating the inversion recovery T_1 values. The Bloch simulations indicated that incomplete spoiling and inaccurate B_1 mapping could account for the observed differences.

42
43
44
45
46
47
48
49
50
51
52

Conclusion: We conclude that the three most common T_1 mapping protocols produce stable T_1 values in phantoms, but not *in vivo*. To improve the accuracy of T_1 mapping, we recommend that sites perform *in vivo* validation of their T_1 mapping method against the inversion recovery reference method, as the first step towards developing a robust calibration scheme.

53
54
55
56
57
58
59
60

Word count for abstract: 262

Keywords: relaxometry, T_1 mapping, quantitative MRI, accuracy, precision, inversion recovery, Look-Locker, variable flip angle, B_1 mapping

References

1. MSSC. <http://www.mssociety.ca/en/information>. MS Society of Canada 2012.
2. Polman CH, Reingold SC, Banwell B, Clanet M, Cohen JA, Filippi M, Fujihara K, Havrdova E, Hutchinson M, Kappos L, Lublin FD, Montalban X, O'Connor P, Sandberg-Wollheim M, Thompson AJ, Waubant E, Weinshenker B, Wolinsky JS. Diagnostic criteria for multiple sclerosis: 2010 revisions to the McDonald criteria. *Ann Neurol* 2011;69(2):292-302.
3. Frohman EM, Racke MK, Raine CS. Multiple sclerosis--the plaque and its pathogenesis. *The New England journal of medicine* 2006;354(9):942-955.
4. McFarland HF, Martin R. Multiple sclerosis: a complicated picture of autoimmunity. *Nature immunology* 2007;8(9):913-919.
5. Noseworthy JH, Lucchinetti C, Rodriguez M, Weinshenker BG. Multiple sclerosis. *The New England journal of medicine* 2000;343(13):938-952.
6. Peterson JW, Bo L, Mork S, Chang A, Trapp BD. Transected neurites, apoptotic neurons, and reduced inflammation in cortical multiple sclerosis lesions. *Ann Neurol* 2001;50(3):389-400.
7. Schmierer K, Thavarajah JR, An SF, Brandner S, Miller DH, Tozer DJ. Effects of formalin fixation on magnetic resonance indices in multiple sclerosis cortical gray matter. *Journal of magnetic resonance imaging : JMRI* 2010;32(5):1054-1060.
8. Stadelmann C, Albert M, Wegner C, Bruck W. Cortical pathology in multiple sclerosis. *Current opinion in neurology* 2008;21(3):229-234.
9. Perry VH, Anthony DC. Axon damage and repair in multiple sclerosis. *Philosophical transactions of the Royal Society of London Series B, Biological sciences* 1999;354(1390):1641-1647.
10. Lassmann H. Axonal and neuronal pathology in multiple sclerosis: What have we learnt from animal models. *Experimental neurology* 2010;225(1):2-8.
11. Staigaitis SM, Chang A, Trapp BD. Cortical pathology in multiple sclerosis: experimental approaches to studies on the mechanisms of demyelination and remyelination. *Acta Neurologica Scandinavica* 2012;126:97-102.
12. Klaver R, De Vries HE, Schenk GJ, Geurts JJ. Grey matter damage in multiple sclerosis: A pathology perspective. *Prion* 2013;7(1).
13. Brownell B, Hughes JT. The distribution of plaques in the cerebrum in multiple sclerosis. *Journal of neurology, neurosurgery, and psychiatry* 1962;25:315-320.
14. Calabrese M, Agosta F, Rinaldi F, Mattisi I, Grossi P, Favaretto A, Atzori M, Bernardi V, Barachino L, Rinaldi L, Perini P, Gallo P, Filippi M. Cortical Lesions and Atrophy Associated With Cognitive Impairment in Relapsing-Remitting Multiple Sclerosis. *Archives of neurology* 2009;66(9):1144-1150.
15. Simon JH, Li D, Traboulsee A, Coyle PK, Arnold DL, Barkhof F, Frank JA, Grossman R, Paty DW, Radue EW, Wolinsky JS. Standardized MR imaging protocol for multiple sclerosis: Consortium of MS Centers consensus guidelines. *AJNR American journal of neuroradiology* 2006;27(2):455-461.
16. Schmierer K, Scaravilli F, Altmann DR, Barker GJ, Miller DH. Magnetization transfer ratio and myelin in postmortem multiple sclerosis brain. *Ann Neurol* 2004;56(3):407-415.
17. Schmierer K, Tozer DJ, Scaravilli F, Altmann DR, Barker GJ, Tofts PS, Miller DH. Quantitative magnetization transfer imaging in postmortem multiple sclerosis brain. *Journal of magnetic resonance imaging : JMRI* 2007;26(1):41-51.

18. Levesque I, Sled JG, Narayanan S, Santos AC, Brass SD, Francis SJ, Arnold DL, Pike GB. The role of edema and demyelination in chronic T-1 black holes: A quantitative magnetization transfer study. *Journal of Magnetic Resonance Imaging* 2005;21(2):103-110.
19. Levesque IR, Giacomini PS, Narayanan S, Ribeiro LT, Sled JG, Arnold DL, Pike GB. Quantitative magnetization transfer and myelin water imaging of the evolution of acute multiple sclerosis lesions. *Magnetic resonance in medicine : official journal of the Society of Magnetic Resonance in Medicine / Society of Magnetic Resonance in Medicine* 2010;63(3):633-640.
20. Tardif CL, Bedell BJ, Eskildsen SF, Collins DL, Pike GB. Quantitative Magnetic Resonance Imaging of Cortical Multiple Sclerosis Pathology. *Multiple Sclerosis International* 2012;2012:13.
21. Arnold DL, Matthews PM. MRI in the diagnosis and management of multiple sclerosis. *Neurology* 2002;58(8 suppl 4):S23-S31.
22. Anderson VM, Fox NC, Miller DH. Magnetic resonance imaging measures of brain atrophy in multiple sclerosis. *Journal of Magnetic Resonance Imaging* 2006;23(5):605-618.
23. De Stefano N, Battaglini M, Smith SM. Measuring Brain Atrophy in Multiple Sclerosis. *Journal of Neuroimaging* 2007;17:10S-15S.
24. Sepulcre J, Goni J, Masdeu JC, Bejarano B, de Mendizabal NV, Toledo JB, Villoslada P. Contribution of White Matter Lesions to Gray Matter Atrophy in Multiple Sclerosis. *Archives of neurology* 2009;66(2):173-179.
25. Derakhshan M, Caramanos Z, Giacomini PS, Narayanan S, Maranzano J, Francis SJ, Arnold DL, Collins DL. Evaluation of automated techniques for the quantification of grey matter atrophy in patients with multiple sclerosis. *NeuroImage* 2010;52(4):1261-1267.
26. Filippi M, Agosta F. Magnetic resonance techniques to quantify tissue damage, tissue repair, and functional cortical reorganization in multiple sclerosis. *Progress in brain research* 2009;175:465-482.
27. Kidd D, Barkhof F, McConnell R, Algra PR, Allen IV, Revesz T. Cortical lesions in multiple sclerosis. *Brain : a journal of neurology* 1999;122 (Pt 1):17-26.
28. Bedell BJ, Narayana PA. Implementation and evaluation of a new pulse sequence for rapid acquisition of double inversion recovery images for simultaneous suppression of white matter and CSF. *Journal of magnetic resonance imaging : JMRI* 1998;8(3):544-547.
29. Filippi M, Rocca MA. Multiple sclerosis and allied white matter diseases. *Neurological sciences : official journal of the Italian Neurological Society and of the Italian Society of Clinical Neurophysiology* 2008;29 Suppl 3:319-322.
30. Savadjiev P, Campbell JS, Pike GB, Siddiqi K. 3D curve inference for diffusion MRI regularization and fibre tractography. *Medical image analysis* 2006;10(5):799-813.
31. MamayyezSiahka P, Campbell JSW, Savadjiev P, Pike GB, Siddiqi K. Beyond crossing fibres: Probabilistic tractography of complex subvoxel fibre geometries. *MICCAI Workshop on Diffusion Modelling 2009*.
32. Wedeen VJ, Hagmann P, Tseng WY, Reese TG, Weisskoff RM. Mapping complex tissue architecture with diffusion spectrum magnetic resonance imaging. *Magnetic resonance in medicine : official journal of the Society of Magnetic Resonance in Medicine / Society of Magnetic Resonance in Medicine* 2005;54(6):1377-1386.
33. Wedeen VJ, Wang RP, Schmahmann JD, Benner T, Tseng WYI, Dai G, Pandya DN, Hagmann P, D'Arceuil H, de Crespigny AJ. Diffusion spectrum magnetic resonance imaging (DSI) tractography of crossing fibers. *NeuroImage* 2008;41(4):1267-1277.

34. Pagani E, Bammer R, Horsfield MA, Rovaris M, Gass A, Ciccarelli O, Filippi M. Diffusion MR imaging in multiple sclerosis: technical aspects and challenges. *AJNR American journal of neuroradiology* 2007;28(3):411-420.
35. Schmierer K, Wheeler-Kingshott CA, Boulby PA, Scaravilli F, Altmann DR, Barker GJ, Tofts PS, Miller DH. Diffusion tensor imaging of post mortem multiple sclerosis brain. *NeuroImage* 2007;35(2):467-477.
36. Calabrese M, Rinaldi F, Seppi D, Favaretto A, Squarcina L, Mattisi I, Perini P, Bertoldo A, Gallo P. Cortical diffusion-tensor imaging abnormalities in multiple sclerosis: a 3-year longitudinal study. *Radiology* 2011;261(3):891-898.
37. Wolff SD, Balaban RS. Magnetization transfer contrast (MTC) and tissue water proton relaxation in vivo. *Magnetic resonance in medicine : official journal of the Society of Magnetic Resonance in Medicine / Society of Magnetic Resonance in Medicine* 1989;10(1):135-144.
38. Henkelman RM, Huang X, Xiang QS, Stanisz GJ, Swanson SD, Bronskill MJ. Quantitative interpretation of magnetization transfer. *Magnetic resonance in medicine : official journal of the Society of Magnetic Resonance in Medicine / Society of Magnetic Resonance in Medicine* 1993;29(6):759-766.
39. Graham SJ, Henkelman RM. Understanding pulsed magnetization transfer. *Journal of magnetic resonance imaging : JMRI* 1997;7(5):903-912.
40. Henkelman RM, Stanisz GJ, Graham SJ. Magnetization transfer in MRI: a review. *NMR in biomedicine* 2001;14(2):57-64.
41. Ge Y, Kolson DL, Babb JS, Mannon LJ, Grossman RI. Whole brain imaging of HIV-infected patients: quantitative analysis of magnetization transfer ratio histogram and fractional brain volume. *AJNR American journal of neuroradiology* 2003;24(1):82-87.
42. Dousset V, Armand JP, Huot P, Viaud B, Caille JM. Magnetization transfer imaging in AIDS-related brain diseases. *Neuroimaging clinics of North America* 1997;7(3):447-460.
43. Wu Y, Storey P, Carrillo A, Saglamer C, Cohen BA, Epstein LG, Edelman RR, Ragin AB. Whole brain and localized magnetization transfer measurements are associated with cognitive impairment in patients infected with human immunodeficiency virus. *AJNR American journal of neuroradiology* 2008;29(1):140-145.
44. Fornari E, Maeder P, Meuli R, Ghika J, Knyazeva MG. Demyelination of superficial white matter in early Alzheimer's disease: a magnetization transfer imaging study. *Neurobiology of aging* 2012;33(2):428 e427-419.
45. Giulietti G, Bozzali M, Figura V, Spano B, Perri R, Marra C, Lacidogna G, Giubilei F, Caltagirone C, Cercignani M. Quantitative magnetization transfer provides information complementary to grey matter atrophy in Alzheimer's disease brains. *Neuroimage* 2012;59(2):1114-1122.
46. Ridha BH, Tozer DJ, Symms MR, Stockton KC, Lewis EB, Siddique MM, MacManus DG, Rossor MN, Fox NC, Tofts PS. Quantitative magnetization transfer imaging in Alzheimer disease. *Radiology* 2007;244(3):832-837.
47. Wiest R, Burren Y, Hauf M, Schroth G, Pruessner J, Zbinden M, Cattapan-Ludewig K, Kiefer C. Classification of mild cognitive impairment and Alzheimer disease using model-based MR and magnetization transfer imaging. *AJNR American journal of neuroradiology* 2013;34(4):740-746.
48. Li X, Majumdar S. Quantitative MRI of articular cartilage and its clinical applications. *Journal of magnetic resonance imaging : JMRI* 2013;38(5):991-1008.

49. Stikov N, Keenan KE, Pauly JM, Smith RL, Dougherty RF, Gold GE. Cross-relaxation imaging of human articular cartilage. *Magnetic resonance in medicine : official journal of the Society of Magnetic Resonance in Medicine / Society of Magnetic Resonance in Medicine* 2011;66(3):725-734.
50. Sled JG, Pike GB. Quantitative imaging of magnetization transfer exchange and relaxation properties in vivo using MRI. *Magnetic resonance in medicine : official journal of the Society of Magnetic Resonance in Medicine / Society of Magnetic Resonance in Medicine* 2001;46(5):923-931.
51. Yarnykh VL. Pulsed Z-spectroscopic imaging of cross-relaxation parameters in tissues for human MRI: theory and clinical applications. *Magnetic resonance in medicine : official journal of the Society of Magnetic Resonance in Medicine / Society of Magnetic Resonance in Medicine* 2002;47(5):929-939.
52. Cercignani M, Alexander DC. Optimal acquisition schemes for in vivo quantitative magnetization transfer MRI. *Magnetic resonance in medicine : official journal of the Society of Magnetic Resonance in Medicine / Society of Magnetic Resonance in Medicine* 2006;56(4):803-810.
53. Portnoy S, Stanisz GJ. Modeling pulsed magnetization transfer. *Magnetic resonance in medicine : official journal of the Society of Magnetic Resonance in Medicine / Society of Magnetic Resonance in Medicine* 2007;58(1):144-155.
54. Ramani A, Dalton C, Miller DH, Tofts PS, Barker GJ. Precise estimate of fundamental in-vivo MT parameters in human brain in clinically feasible times. *Magnetic resonance imaging* 2002;20(10):721-731.
55. Levesque IR, Sled JG, Narayanan S, Giacomini PS, Ribeiro LT, Arnold DL, Pike GB. Reproducibility of quantitative magnetization-transfer imaging parameters from repeated measurements. *Magnetic resonance in medicine : official journal of the Society of Magnetic Resonance in Medicine / Society of Magnetic Resonance in Medicine* 2010;64(2):391-400.
56. Levesque IR, Sled JG, Pike GB. Iterative optimization method for design of quantitative magnetization transfer imaging experiments. *Magnetic resonance in medicine : official journal of the Society of Magnetic Resonance in Medicine / Society of Magnetic Resonance in Medicine* 2011;66(3):635-643.
57. Yarnykh VL. Fast macromolecular proton fraction mapping from a single off-resonance magnetization transfer measurement. *Magnetic resonance in medicine : official journal of the Society of Magnetic Resonance in Medicine / Society of Magnetic Resonance in Medicine* 2012;68(1):166-178.
58. Underhill HR, Rostomily RC, Mikheev AM, Yuan C, Yarnykh VL. Fast bound pool fraction imaging of the in vivo rat brain: association with myelin content and validation in the C6 glioma model. *NeuroImage* 2011;54(3):2052-2065.
59. Gloor M, Scheffler K, Bieri O. Quantitative magnetization transfer imaging using balanced SSFP. *Magnetic resonance in medicine : official journal of the Society of Magnetic Resonance in Medicine / Society of Magnetic Resonance in Medicine* 2008;60(3):691-700.
60. Lustig M, Donoho D, Pauly JM. Sparse MRI: The application of compressed sensing for rapid MR imaging. *Magnetic resonance in medicine : official journal of the Society of Magnetic Resonance in Medicine / Society of Magnetic Resonance in Medicine* 2007;58(6):1182-1195.
61. Gamper U, Boesiger P, Kozerke S. Compressed sensing in dynamic MRI. *Magnetic resonance in medicine : official journal of the Society of Magnetic Resonance in Medicine / Society of Magnetic Resonance in Medicine* 2008;59(2):365-373.

62. Menzel MI, Tan ET, Khare K, Sperl JI, King KF, Tao XD, Hardy CJ, Marinelli L. Accelerated Diffusion Spectrum Imaging in the Human Brain Using Compressed Sensing. *Magnetic Resonance in Medicine* 2011;66(5):1226-1233.
63. Doneva M, Bornert P, Eggers H, Stehning C, Senegas J, Mertins A. Compressed sensing reconstruction for magnetic resonance parameter mapping. *Magnetic resonance in medicine : official journal of the Society of Magnetic Resonance in Medicine / Society of Magnetic Resonance in Medicine* 2010;64(4):1114-1120.
64. Li W, Griswold M, Yu X. Fast cardiac T(1) mapping in mice using a model-based compressed sensing method. *Magnetic resonance in medicine : official journal of the Society of Magnetic Resonance in Medicine / Society of Magnetic Resonance in Medicine* 2011.
65. Sumpf TJ, Uecker M, Boretius S, Frahm J. Model-Based Nonlinear Inverse Reconstruction for T2 Mapping Using Highly Undersampled Spin-Echo MRI. *Journal of Magnetic Resonance Imaging* 2011;34(2):420-428.
66. Ji SH, Xue Y, Carin L. Bayesian compressive sensing. *Ieee T Signal Proces* 2008;56(6):2346-2356.
67. Bilgic B, Goyal VK, Adalsteinsson E. Multi-contrast reconstruction with Bayesian compressed sensing. *Magnetic resonance in medicine : official journal of the Society of Magnetic Resonance in Medicine / Society of Magnetic Resonance in Medicine* 2011;66(6):1601-1615.
68. Lustig M, Pauly JM. SPIRiT: Iterative self-consistent parallel imaging reconstruction from arbitrary k-space. *Magnetic resonance in medicine : official journal of the Society of Magnetic Resonance in Medicine / Society of Magnetic Resonance in Medicine* 2010;64(2):457-471.
69. Uecker M, Lai P, Murphy MJ, Virtue P, Elad M, Pauly JM, Vasanawala SS, Lustig M. ESPIRiT—an eigenvalue approach to autocalibrating parallel MRI: Where SENSE meets GRAPPA. *Magnetic Resonance in Medicine* 2013;n/a-n/a.
70. Weller DS, Polimeni JR, Grady L, Wald LL, Adalsteinsson E, Goyal VK. Combined Compressed Sensing and Parallel Mri Compared for Uniform and Random Cartesian Undersampling of K-Space. *2011 Ieee International Conference on Acoustics, Speech, and Signal Processing* 2011:553-556.
71. She H, Chen R-R, Liang D, DiBella EVR, Ying L. Sparse BLIP: BLind Iterative Parallel imaging reconstruction using compressed sensing. *Magnetic Resonance in Medicine* 2013;n/a-n/a.
72. Wu B, Millane RP, Watts R, Bones PJ. Prior estimate-based compressed sensing in parallel MRI. *Magnetic resonance in medicine : official journal of the Society of Magnetic Resonance in Medicine / Society of Magnetic Resonance in Medicine* 2011;65(1):83-95.
73. Chang CH, Ji J. Compressed Sensing MRI with Multichannel Data Using Multicore Processors. *Magnetic Resonance in Medicine* 2010;64(4):1135-1139.
74. Liang D, Liu B, Wang JJ, Ying L. Accelerating SENSE Using Compressed Sensing. *Magnetic Resonance in Medicine* 2009;62(6):1574-1584.
75. Liu B, Zou YM, Ying L. SparseSENSE: Application of compressed sensing in parallel MRI. *2008 International Special Topic Conference on Information Technology and Applications in Biomedicine, Vols 1 and 2* 2008:261-264.
76. Ji JX, Zhao C, Lang T. Compressed Sensing Parallel Magnetic Resonance Imaging. *2008 30th Annual International Conference of the IEEE Engineering in Medicine and Biology Society, Vols 1-8* 2008:1671-1674.
77. Yarnykh VL. Optimal radiofrequency and gradient spoiling for improved accuracy of T1 and B1 measurements using fast steady-state techniques. *Magnetic resonance in medicine : official*

- journal of the Society of Magnetic Resonance in Medicine / Society of Magnetic Resonance in Medicine 2010;63(6):1610-1626.
78. Yarnykh VL. Actual flip-angle imaging in the pulsed steady state: a method for rapid three-dimensional mapping of the transmitted radiofrequency field. *Magnetic resonance in medicine : official journal of the Society of Magnetic Resonance in Medicine / Society of Magnetic Resonance in Medicine* 2007;57(1):192-200.
79. Sacolick LI, Wiesinger F, Hancu I, Vogel MW. B1 mapping by Bloch-Siegert shift. *Magnetic resonance in medicine : official journal of the Society of Magnetic Resonance in Medicine / Society of Magnetic Resonance in Medicine* 2010;63(5):1315-1322.
80. Tardif CLS, N.; Levesque, I.R.; Pike, G.B. Impact of Three B1 Mapping Techniques on Variable Flip Angle T1 Measurements. *Proc Intl Soc Mag Reson Med* 2011;19.
81. Zhang T, Pauly J, Levesque I. Accelerating Parameter Mapping with a Locally Low Rank Constraint. In Proceedings of the 21st Annual Meeting of ISMRM 2013:p.2458.